Sustainable Chemistry and Pharmacy 52 (2026) 102475

Contents lists available at ScienceDirect

Sustainable Chemistry and Pharmacy

journal homepage: www.elsevier.com/locate/scp

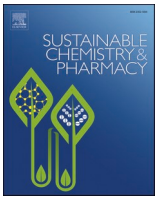

Ionic liquid-based sample pretreatment platforms: comparing solid supports and aqueous biphasic systems for enhanced bioanalytical performance

Maria S.M. Mendes, Hugo Santos, Inês Cruz, Márcia C. Neves, Mara G. Freire *, Francisca A. e Silva **

CICECO – Aveiro Institute of Materials, Department of Chemistry, University of Aveiro, Aveiro, Portugal

ARTICLE INFO

Keywords:
Sample pretreatment
Aqueous biphasic system
Solid-phase extraction
Ionic liquid

ABSTRACT

Reliable biomarker analysis in human serum is a critical bioanalytical task supporting disease detection and management. However, conventional serum pretreatment methods often fail to remove high-abundance proteins without analyte loss, potentially leading to false results, or rely on resource-intensive workflows poorly aligned with green analytical practices. Ionic liquids provide a versatile enabling technology, offering tunable interactions for selective protein depletion and enhanced biomarker recovery. In this work, their dual role in serum pretreatment is exploited through two complementary configurations, namely solid-phase extraction, where ionic liquids act as immobilized ligands, and aqueous biphasic systems, where they function as phase-forming agents. Both approaches were compared using Green Sample Preparation metrics to evaluate operational efficiency and environmental performance at the analytical level. Solid-phase extraction achieved >92% protein depletion with 89% biomarker recovery. This approach also reduced sample consumption and waste generation, demonstrating strong bioanalytical performance alongside improved alignment with Green Analytical Chemistry principles.

1. Introduction

Screening strategies based on circulating protein biomarkers have significantly contributed to earlier detection and improved clinical management of various diseases (Wang et al., 2023). However, high-abundance proteins such as human serum albumin (HSA) and immunoglobulin G (IgG) frequently interfere with the detection of low-concentration biomarkers in human serum, making their selective depletion a critical step in accurate bioanalytical workflows (Issaq and Veenstra, 2020). Routine serum pretreatment methods include solid-phase extraction (SPE), protein precipitation and liquid-liquid extraction (LLE) (Issaq and Veenstra, 2020). SPE uses functionalized sorbents, such as antibodies, protein A/G, or ion-exchange ligands, for the selective retention or depletion of specific proteins (Issaq and Veenstra, 2020). In contrast, protein precipitation induces the aggregation and separation of proteins using organic solvents, salts, or acids (Issaq and Veenstra, 2020). LLE is based on the differential partition of analytes between two immiscible phases, typically involving a water-immiscible organic solvent (Issaq and Veenstra, 2020). Although SPE provides superior selectivity

* Corresponding author.
** Corresponding author.
E-mail addresses: maragfreire@ua.pt (M.G. Freire), francisca.silva@ua.pt (F.A. e Silva).

https://doi.org/10.1016/j.scp.2026.102475
Received 6 April 2026; Received in revised form 26 May 2026; Accepted 12 June 2026

and effective removal of high-abundance proteins, it requires higher technical and financial investment (Issaq and Veenstra, 2020). Conversely, precipitation and LLE are more accessible and cost-effective but are generally less selective, less aligned with reduced resource consumption approaches in analytical workflows, and prone to co-precipitation or loss of target analytes (Issaq and Veenstra, 2020).

Considering the limitations associated with conventional sample pretreatment techniques, the principles of Green Analytical Chemistry advocate the development of more efficient analytical workflows with reduced environmental impact (Gałuszka et al., 2013). Within Green Sample Preparation, the focus lies on minimizing the environmental footprint of analytical procedures by reducing solvent consumption and replacing conventional reagents with less hazardous or less resource-intensive alternatives, while maintaining analytical performance (López-Lorente et al., 2022). In this context, ionic liquids (ILs) arise as versatile agents, offering tunable physicochemical properties through rational design (Zeger et al., 2025). By enabling selective interactions with biomolecules in complex biological matrices, ILs provide a suitable platform for advanced sample pretreatment (González-Martín et al., 2023a). ILs have been employed as phase-forming agents in aqueous biphasic systems (ABS), a water-based LLE strategy that enables efficient depletion of high-abundance serum proteins and biomarker recovery (Rosa et al., 2023). Beyond their application as liquid extraction media, ILs can also be immobilized onto solid supports through supported ionic liquids (SILs), in which IL moieties are covalently attached to biocompatible, low-cost silica materials (Bernardo et al., 2020). This approach retains IL selectivity and tunability while mitigating common drawbacks of their liquid state, including handling challenges and incompatibility with some analytical techniques (Bernardo et al., 2020; Mota-Martinez et al., 2018). Ultimately, these developments are consistent with the United Nations Sustainable Development Goals (SDGs 3, 9 and 12), which relate to improved health outcomes, technological innovation, and responsible resource use.

While SILs are emerging tools in bioseparation (Capela et al., 2023), their application in sample pretreatment strategies for bioanalysis remains limited, whereas IL-based ABS have already been reported for these purposes (Rosa et al., 2023). This highlights the still underexplored versatility of ILs as platforms for engineering bioanalytical interfaces. Leveraging this potential, this work

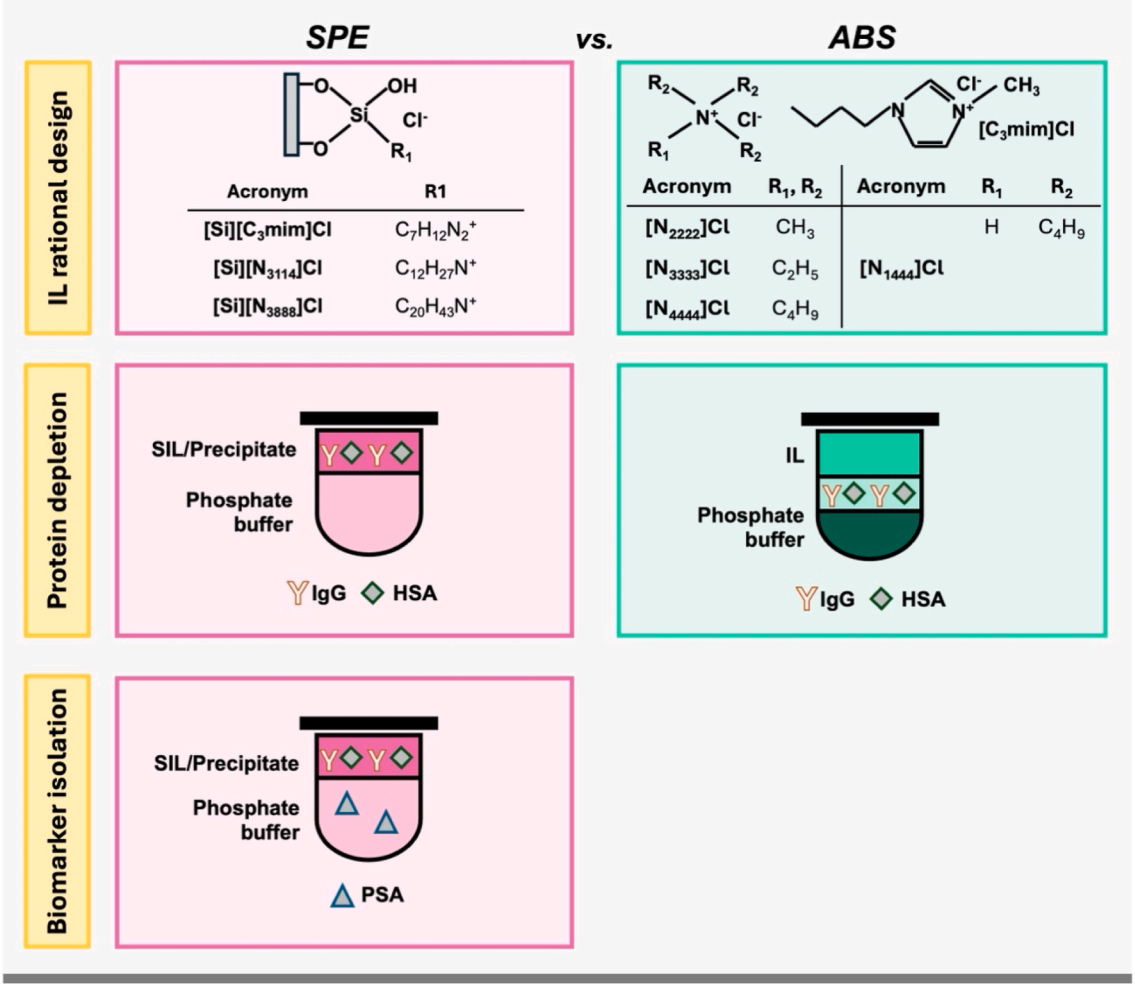

Fig. 1. Strategy employed for the development and optimization of human serum pretreatment via IL-based SPE and ABS.

demonstrates, for the first time, the dual role of ILs in human serum pretreatment by exploiting their ability to operate in two distinct configurations: as immobilized ligands in SPE and as phase-forming agents in ABS. ABS rely on liquid-liquid partition and interfacial precipitation phenomena driven by phase-forming components, whereas SIL-based SPE employs surface-confined IL moieties as affinity ligands to tune protein-sorbent interactions. The two IL-based strategies were critically compared regarding high-abundance protein depletion, target biomarker isolation, and environmental performance under the same biological and analytical context. Green Sample Preparation metrics (AGREEprep and SPMS) were further applied to assess environmental impact and operational efficiency. Overall, this work identifies the best-performing IL-based strategy for bioanalytical applications, as illustrated in Fig. 1.

2. Materials and methods

2.1. Materials

To investigate the SPE configuration for serum pretreatment, three distinct SILs were synthesized: silica functionalized with 1-methyl-3-propylimidazolium chloride ([Si][C_3mim]Cl), silica functionalized with propyldimethylbutylammonium chloride ([Si][N_{3114}]Cl), and silica functionalized with propyltrioctylammonium chloride ([Si][N_{3888}]Cl). The chemicals used for their synthesis included silica gel (60 Å, particle size of 0.2-0.5 nm) from Merck, and the following solvents: toluene (99.98 wt% purity), ethanol (99.99 wt% purity), and methanol (99.98 wt% purity) from Fisher Scientific. Additional reagents included (3-chloropropyl)trimethoxysilane (98 wt% purity) and *N*-methylimidazole (99 wt% purity) from Acros Organics, and *N,N*-dimethylbutylamine (99 wt% purity) and trioctylamine (>98 wt% purity) from Sigma-Aldrich.

To generate ABS, the following ILs were used: tetraethylammonium chloride ([N_{2222}]Cl, >98 wt% purity from Sigma-Aldrich), tetrapropylammonium chloride ([N_{3333}]Cl, >99 wt% purity from Alfa Aesar), tetrabutylammonium chloride ([N_{4444}]Cl, >97 wt% purity from Sigma Aldrich), 1-methyl-3-propylimidazolium chloride ([C_3mim]Cl, >98 wt% purity from iolitec) and tributylmethylammonium chloride ([N_{1444}]Cl, >97 wt% purity from Sigma Aldrich).

Phosphate-buffered saline (PBS) was prepared by dissolving a Sigma-Aldrich PBS tablet in 200 mL of distilled water, resulting in a solution containing 0.01 M phosphate buffer (monobasic potassium phosphate, KH_2PO_4 and dibasic sodium phosphate, Na_2HPO_4), 0.0027 M potassium chloride (KCl) and 0.137 M sodium chloride (NaCl), with a final pH of 7.4 at 25°C. In turn, a phosphate buffer solution at pH of ca. 7 was prepared with a total salt concentration of 40 wt%, composed of 2.672 M of dibasic potassium phosphate (K_2HPO_4, >98 wt% purity) and 2.012 M of KH_2PO_4 (99.5 wt% purity), both from Sigma-Aldrich. The combined molarity of phosphate species in solution was approximately 4.68 M.

For the high-performance liquid chromatography (HPLC) mobile phase, sodium dihydrogen phosphate monohydrate ($NaH_2PO_4 \cdot H_2O$, 99 wt% purity), dibasic sodium phosphate heptahydrate ($Na_2HPO_4 \cdot 7H_2O$, 99 wt% purity) and NaCl (99.5 wt% purity) from PanReac were used. To prepare IgG and HSA standard solutions, purified human IgG with a concentration of 29.4 mg mL^{-1} was

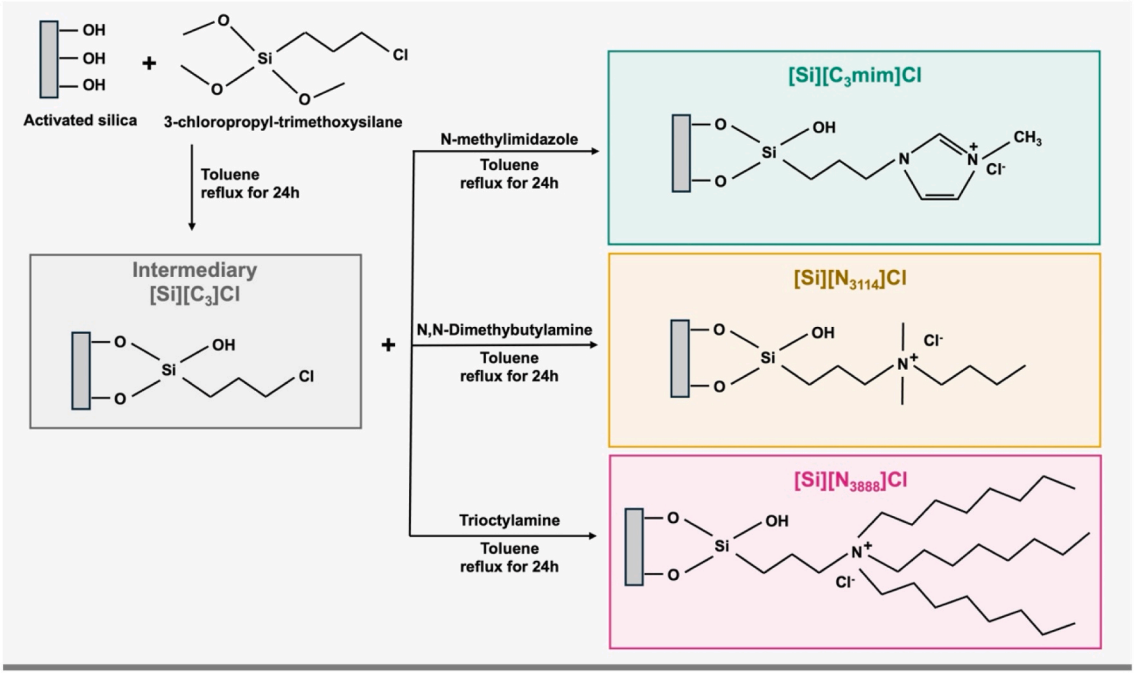

Fig. 2. SIL preparation process and chemical structures, showing the synthesis of the intermediary compound ([Si][C_3]Cl) and the final materials ([Si][C_3mim]Cl, [Si][N_{3114}]Cl and [Si][N_{3888}]Cl).

obtained from Innovative Researched, Inc., stored at −80°C, while lyophilized human serum albumin powder with ≥97 wt% purity was acquired from Sigma-Aldrich, stored at 4°C. Commercial human serum (male AB plasma, Sigma-Aldrich, H4522) was used as the biological matrix and stored at −20°C until use. The commercial human prostate-specific antigen (PSA)-total enzyme-linked immunosorbent assay (ELISA) kit (RAB0331) was from Sigma-Aldrich, stored at 4°C.

2.2. Synthesis and characterization of SILs

SILs were synthesized according to Fig. 2, following a method originally proposed in the literature (Qiu et al., 2006), later adapted and validated by our group, as reported in previous works (Capela et al., 2023). The synthesis involved three main steps, namely silica activation, intermediate preparation and functionalization. First, silica was activated with a 37 wt% solution of hydrochloric acid (HCl) for 24 h to increase the content of silanol groups on its surface. After activation, silica was washed with 2 L of distilled water until the wash water reached pH 7 and then dried in an oven at 60°C for 24 h. Next, to prepare the intermediate compound 3-chloropropylsilane ([Si][C_3]Cl), 5 g of activated silica was suspended in 60 mL of toluene along with 5 mL of 3-chloropropyltrimethoxysilane. This mixture was refluxed at 110°C with magnetic stirring for 24 h. The intermediate was subsequently filtered and washed sequentially with 100 mL of toluene, 200 mL of an ethanol-water solution (1:1), 500 mL of distilled water, and 100 mL of methanol, followed by drying for 24 h at room temperature. Finally, precursor functionalization involved the suspension of 5 g of [Si][C_3]Cl in 50 mL of toluene with 5 mL of the required cationic source: *N*-methylimidazole for [Si][C_3mim]Cl, *N,N*-dimethylbutylamine for [Si][N_{3114}]Cl, and trioctylamine for [Si][N_{3888}]Cl. This mixture was refluxed at 110°C with magnetic stirring for another 24 h. The produced SILs were filtered and washed with 100 mL toluene, followed by 350 mL of methanol, 300 mL of distilled water, and 150 mL of methanol, then dried for another 24 h at room temperature.

Carbon, hydrogen, and nitrogen contents (expressed as weight percentages) of [Si][C_3mim]Cl, [Si][N_{3114}]Cl and [Si][N_{3888}]Cl were determined using a TruSpec 630–200–200 CHNS analyser. Approximately 2 mg of each sample was introduced into the analyser, with the combustion furnace set at 1075°C and the afterburner at 850°C. Carbon and hydrogen contents were measured via infrared absorption, while nitrogen was quantified using thermal conductivity.

2.3. Serum pretreatment using SPE

The effectiveness of SPE using the three different SILs for human serum pretreatment was assessed based on their ability to deplete IgG and HSA. Commercial human serum was diluted in distinct buffering systems, including PBS (pH ≈ 7.4) and K_2HPO_4/KH_2PO_4 (pH ≈ 7). Activated silica was studied as a reference material. Each SIL or activated silica sample was placed into 1.5 mL microtubes with a solid-to-liquid (S:L) ratio of 100 mg mL^{-1} (i.e., 50 mg of SIL or activated silica and 0.05 g of human serum diluted 10-fold in the respective buffers). A negative control without activated silica/SIL was also prepared for each buffer. After accurately weighing each component within an accuracy of 10^{-4} g, the systems were left under agitation for 60 min and then centrifuged at 13000 rpm for 20 min. The liquid phases were subsequently collected using syringes, and the concentrations of IgG and HSA were quantified by size-exclusion HPLC (SE-HPLC) using pre-established calibration curves. Prior to SE-HPLC analysis, the liquid phases were diluted 10-fold in the HPLC mobile phase. All experiments were performed in triplicate, and results are expressed as mean ± standard deviation.

To assess the performance of the SILs in depleting proteins from human serum, the depletion efficiencies of IgG and HSA (DE_{IgG}% and DE_{HSA}%, respectively) were calculated using Equations (1) and (2).

$$m_{IgG/HSA}^{Depleted} = m_{IgG/HSA}^{Initial} - m_{IgG/HSA}^{Liquid\ phase} \quad (1)$$

$$DE_{IgG/HSA}\% = \frac{m_{IgG/HSA}^{Depleted}}{m_{IgG/HSA}^{Initial}} \times 100 \quad (2)$$

where $m_{IgG/HSA}^{Depleted}$ corresponds to the mass of IgG or HSA depleted via precipitation or adsorption onto the SIL, whereas $m_{IgG/HSA}^{Initial}$ represents the initial mass of IgG or HSA in the system, and $m_{IgG/HSA}^{Liquid\ phase}$ refers to the mass of IgG or HSA remaining in the liquid phase.

2.4. Serum pretreatment using ABS

To evaluate ABS ability to deplete IgG and HSA via interfacial precipitation, systems composed of 0.3 g of IL plus 0.5 g of K_2HPO_4/KH_2PO_4 buffer plus 0.1 g of human serum plus 0.1 g of water were studied. These biphasic compositions were selected based on the binodal curves of the corresponding systems (Belchior et al., 2020), which included [N_{2222}]Cl, [N_{3333}]Cl, [N_{4444}]Cl, [C_3mim]Cl and [N_{1444}]Cl in combination with a phosphate buffer (K_2HPO_4/KH_2PO_4) at pH ≈ 7.

Binodal curves were determined only for the systems not previously reported in the literature, namely those comprising [C_3mim]Cl and [N_{1444}]Cl (Belchior et al., 2020). These were determined at 25 (±1)°C and atmospheric pressure using the cloud point titration method, as previously described (Areekal et al., 2025). Briefly, aqueous solutions of K_2HPO_4/KH_2PO_4 at pH ≈ 7 at circa 40 wt% and aqueous solutions of each IL with concentrations of circa 80 wt% were prepared. Under continuous stirring, the K_2HPO_4/KH_2PO_4 buffer was added dropwise to the IL solution until the mixture turned cloudy (indicating a biphasic system), followed by dropwise addition of water until a clear monophasic solution was restored. The compositions of the ternary systems after each addition step were determined gravimetrically, with an associated uncertainty of $\pm 10^{-4}$ g.

For the preparation of ABS for serum pretreatment, the appropriate amount of each component was weighed with an uncertainty of 10^{-4} g. For each mixture point, systems were prepared, stirred, and centrifuged at 3500 rpm for 10 min. Then, the top (IL-rich) and bottom (K_2HPO_4/KH_2PO_4-rich) phases were carefully separated using syringes and subsequently diluted 10-fold with the HPLC mobile phase for analysis. All experiments were conducted in triplicate, and results are presented as mean ± standard deviation. The mass of protein depleted in the interphase ($m_{IgG/HSA}^{Depleted}$) was assessed through mass balance (Equation (3)), while the depletion efficiencies of IgG and HSA, DE_{IgG}% and DE_{HSA}%, were determined using Equation (4):

$$m_{IgG/HSA}^{Depleted} = m_{IgG/HSA}^{Initial} - m_{IgG/HSA}^{Top\ phase} - m_{IgG/HSA}^{Bottom\ phase} \tag{3}$$

$$DE_{IgG/HSA}\% = \frac{m_{IgG/HSA}^{Depleted}}{m_{IgG/HSA}^{Initial}} \times 100 \tag{4}$$

where $m_{IgG/HSA}^{Top\ phase}$ and $m_{IgG/HSA}^{Bottom\ phase}$ correspond to the mass of IgG or HSA in the top and bottom phases, respectively, and $m_{IgG/HSA}^{Initial}$ refers to the initial mass of IgG or HSA in the system.

2.5. Chromatographic quantification of IgG and HSA

A Chromaster HPLC system (VWR Hitachi) equipped with a Protein KW-802.5 analytical column (8 mm × 300 mm) and a Protein KW-G 6B guard column, both from Shodex, was used for SE-HPLC quantification of HSA and IgG in each liquid phase obtained after SPE and ABS pretreatment. Depleted proteins were subsequently determined by mass balance, based on the difference between the initial serum protein content and the amount quantified in the liquid phases, as previously described in Equations (1) and (3).

The HPLC mobile phase consisted of a 50 mM sodium phosphate buffer (NaH_2PO_4/Na_2HPO_4) containing 0.3 M NaCl and was operated in isocratic mode at a flow rate of 0.5 mL min^{-1} for 40 min. The column oven and autosampler were maintained at 25°C and 10°C, respectively. Sample injections were set at 25 μL, and detection was carried out using a diode array detector at 280 nm. Under these conditions, IgG and HSA eluted at approximately 15 and 16 min, respectively, with no detectable interference from the sample pretreatment components, as confirmed by the analysis of systems without serum. Quantification of HSA and IgG in each phase was carried out using previously established calibration curves within the 0.1–1.0 mg mL^{-1} range ($R^2 \geq 0.99$).

In combination with the mass balance approach, SE-HPLC with UV detection provides a reliable means of determining protein depletion, while considering potential analyte loss, phase cross-contamination and incomplete phase recovery during sample processing. This analytical approach has been previously validated and demonstrated to provide accurate quantification under the experimental conditions used (Rosa et al., 2023).

2.6. Proof of concept: biomarker isolation using SPE

Following the evaluation of different sample pretreatment configurations for the depletion of IgG and HSA, which identified SIL-based SPE as the most promising, this approach was applied to isolate PSA from human serum in the liquid phase as a proof of concept. For this purpose, the same experimental conditions (i.e., S:L ratio, contact time and centrifugation) as well as separation procedures previously described were employed, this time with commercial human serum spiked with 4 ng mL^{-1} of PSA (the minimum clinically relevant concentration for this serum biomarker (Descotes, 2019)). The PSA concentration in the liquid phase was quantified using PSA ELISA kits according to the manufacturer's protocol, using a calibration curve previously established within the 10.24–200 pg mL^{-1} range ($R^2 \geq 0.99$). The calibration curve, including the LOD (14.98 pg mL^{-1}) and LOQ (44.94 pg mL^{-1}), is shown in Fig. S1 in the Supplementary Material. All experiments were undertaken in triplicate, and results are reported as mean ± standard deviation. To examine possible matrix contributions or endogenous interference in the ELISA response, systems containing pristine human serum (without PSA spiking) were also analysed.

The recovery yields of PSA in the liquid phase and corresponding relative errors of analysis, denoted as $RY_{PSA}^{Liquid\ phase}$% and RE%, respectively, were calculated based on the equations provided below:

$$RY_{PSA}^{Liquid\ phase}\% = \frac{m_{PSA}^{Liquid\ phase}}{m_{PSA}^{Initial}} \times 100 \tag{5}$$

$$RE\% = \frac{m_{PSA}^{Liquid\ phase} - m_{PPSA}^{Initial}}{m_{PSA}^{Initial}} \times 100 \tag{6}$$

where $m_{PSA}^{Liquid\ phase}$ represents the mass of PSA remaining in the liquid phase, $m_{PSA}^{Solid\ phase}$ refers to the mass of PSA in the solid phase, and $m_{PSA}^{Initial}$ corresponds the initial mass of PSA present in the spiked human serum.

2.7. Statistical analysis

Analytical performance data obtained for the different IL-based strategies were statistically analysed using GraphPad Prism

software (GraphPad Software, San Diego, CA, USA). One-way ANOVA followed by Tukey's post hoc multiple comparisons test was applied to determine significant differences between systems ($p < 0.05$). Results are presented using letter-based grouping, where different letters indicate statistically significant differences.

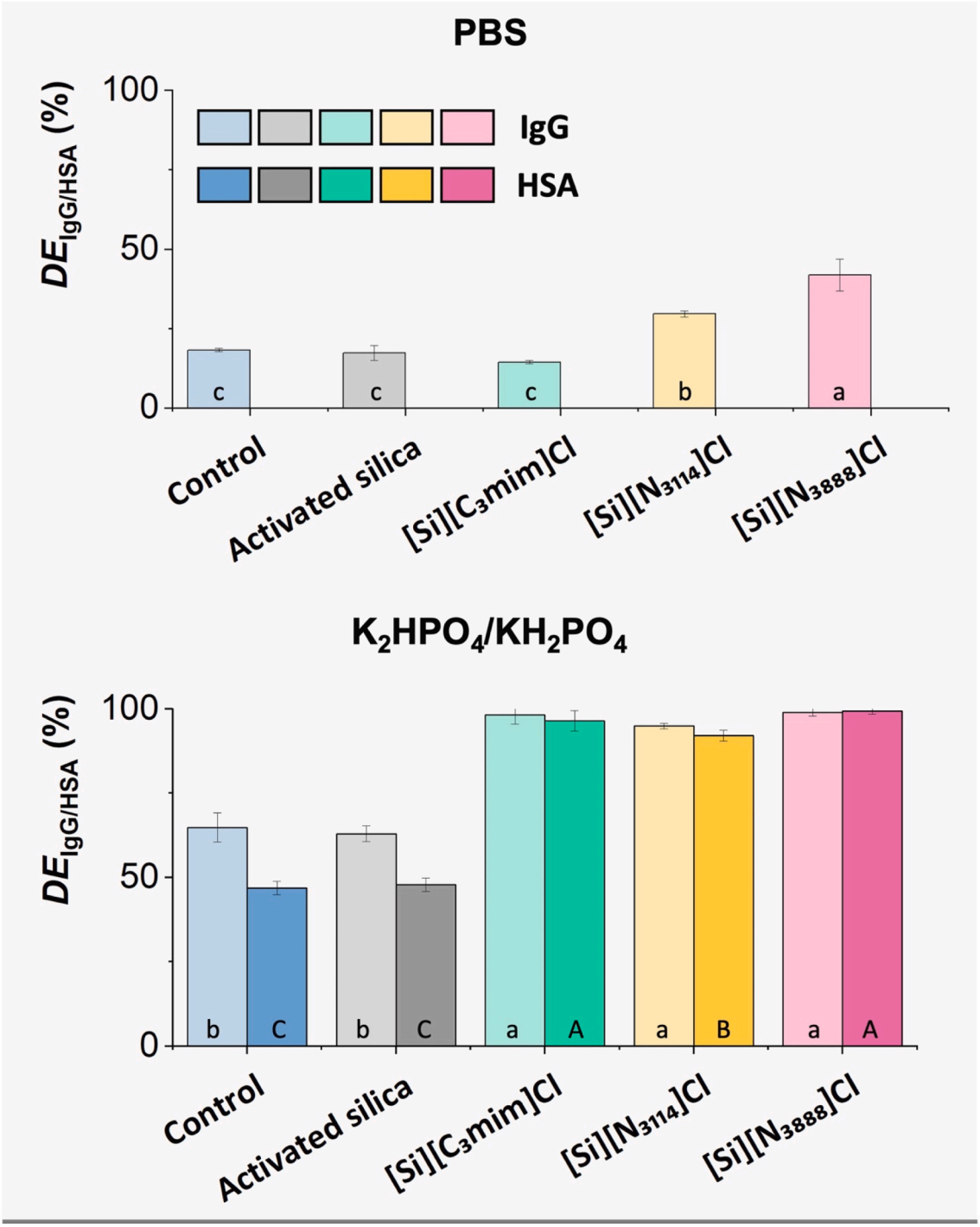

Fig. 3. Depletion efficiencies of IgG (DE_{IgG}, light bars) and HSA (DE_{HSA}, dark bars) obtained via SPE at a solid-to-liquid ratio of 100 mg mL^{-1} with 10-fold diluted human serum, employing two distinct buffering systems, PBS and K_2HPO_4/KH_2PO_4 buffer. Control experiments were performed in the absence of silica and SILs. Bars represent mean values, and error bars indicate standard deviation ($n = 3$). Different lowercase letters (IgG) and uppercase letters (HSA) denote statistically significant differences ($p < 0.05$).

2.8. Circular dichroism

Circular dichroism (CD) spectra were recorded to evaluate the conformational stability of PSA by detecting changes in its secondary structure. CD spectra of PSA were obtained from the liquid phases collected from the most representative SIL system using human serum spiked with 4 ng mL^{-1} of PSA, which was diluted in K_2HPO_4/KH_2PO_4 buffer (4.68 M, pH ≈ 7). A solution of human serum spiked with 4 ng mL^{-1} of PSA in PBS served as reference. CD analyses were also conducted for blank controls to account for any potential influences from the SPE system components. The CD spectra were recorded using a JASCO J-815 spectropolarimeter (JASCO, Easton, MD, USA) at 25°C in rectangular quartz Suprasil CD cuvettes with a path length of 0.1 cm. Each spectrum was generated by averaging three scans collected data in the 190–280 nm range at a scan speed of 50 nm min^{-1}.

3. Results and discussion

To establish the IL-based serum pretreatment platform, SIL-based SPE and IL-based ABS were experimentally evaluated and compared in terms of protein depletion efficiency, biomarker recovery, and environmental impact. SIL-based SPE was first applied to commercial human serum as a complex biological matrix. Three SILs were investigated: [Si][C_3mim]Cl, [Si][N_{3114}]Cl and [Si][N_{3888}]Cl, selected to evaluate the influence of IL cation structure and alkyl chain length on serum protein depletion. The imidazolium-based SIL [Si][C_3mim]Cl was included due to the ability of imidazolium cations to promote electrostatic, hydrophobic and π-π interactions with proteins, while remaining compatible with aqueous biological matrices. The quaternary ammonium-based SILs [Si][N_{3114}]Cl and [Si][N_{3888}]Cl were used to assess the effect of increasing alkyl chain length and hydrophobicity, with enhanced contributions from van der Waals interactions expected particularly for the longer chain [Si][N_{3888}]Cl. Chloride was deliberately chosen as a counterion in line with Green Analytical Chemistry principles (López-Lorente et al., 2022). Compared to more complex and potentially hazardous anions, chloride eliminates the need for extra anion exchange procedures, streamlining SIL synthesis, reducing production costs, and lowering resource demand at both analytical and synthetic level. Silica was selected as the solid support due to its chemical stability, low cost, high surface area and straightforward functionalization.

All SILs were previously reported (Bernardo et al., 2020; Capela et al., 2023). Here, successful covalent immobilization was confirmed by elemental analysis, with carbon (5.61–9.91%) and nitrogen (0.13–2.22%) contents consistent with literature values (Table S1 in the Supplementary Material) (Bernardo et al., 2020; Capela et al., 2023). The resulting SILs combine aqueous stability and resistance to leaching with low cytotoxicity (Bernardo et al., 2020). Overall, their performance is expected to be governed by tunable protein-surface interactions driven by cation type and alkyl chain length, influencing protein behavior during serum pretreatment.

The depletion of IgG and HSA via SIL-based SPE was evaluated using human serum diluted in two distinct buffering systems: PBS (pH ≈ 7.4, 0.15 M) and K_2HPO_4/KH_2PO_4 buffer (pH ≈ 7, 4.68 M). These buffers, differing primarily in ionic strength, were chosen for their ability to maintain near-neutral pH and promote protein biomarker stability under analytical conditions (Brudar and Hribar-Lee, 2021). The operational pH range used in this work (≈7.0-7.4) lies within the stability window of silica-based materials (typically pH 2-8), whereas strongly alkaline conditions (pH > 8) are known to promote silica dissolution and potential leaching, which may compromise downstream detection (Kirkland et al., 1995). Under the experimental conditions applied, no evidence of material instability or analytical interference was observed.

Fig. 3 presents the depletion efficiencies of IgG and HSA, defined as the removal of high-abundance serum proteins via selective precipitation or adsorption onto the various SILs, with activated silica included for comparison. The corresponding numerical data is provided in the Supplementary Material (Table S2). Serum diluted in each buffer without any solid phase was used as control. According to Fig. 3, [Si][N_{3888}]Cl was the most effective SIL for IgG depletion in PBS (0.15 M), achieving 42 ± 5% removal, followed by [Si][N_{3114}]Cl (30 ± 1%) and [Si][C_3mim]Cl (14 ± 1%), while no depletion of HSA was observed with any SIL. In comparison, non-functionalized activated silica removed only 17 ± 2% of IgG and showed negligible depletion of HSA. The selective removal of IgG can be attributed to its larger molecular weight and tendency to form aggregates, which makes it more prone to precipitation or adsorption compared to HSA, which is less susceptible to these phenomena (Sim et al., 2012; Rosa et al., 2007). This difference, combined with the effect of PBS, likely explains why some IgG was removed in the control experiments despite the absence of SILs. The results further emphasize the influence of the SIL chemical structure on IgG depletion. For example, [Si][C_3mim]Cl, which carries a positive charge at the working pH (point of zero charge [PZC] = 8.9) (Capela et al., 2023), adsorbed fewer IgG than the other SILs. However, its aromatic ring may favor π-π interactions with the aromatic residues, contributing to IgG adsorption (Bernardo et al., 2020; Capela et al., 2023). Conversely, [Si][N_{3888}]Cl has a negatively charged surface at pH 7 (PZC = 6.2), enabling electrostatic interactions with positively charged IgG (isoelectric point [pI] = 9) (Capela et al., 2023). Additionally, the presence of three octyl chains renders [Si][N_{3888}]Cl the most hydrophobic SIL investigated, a feature that enhances its interaction with IgG and contributes to its superior depletion performance. On the other hand, [Si][N_{3114}]Cl, with a PZC of 9.2, is positively charged at pH 7 and repels IgG (Capela et al., 2023). Therefore, the combination of hydrophobicity and favourable electrostatic interactions contributes to the higher adsorption efficiency, and thus depletion, of [Si][N_{3888}]Cl (Bernardo et al., 2020; Capela et al., 2023; Han et al., 2023). In general, changing the immobilized IL cation structure, namely the alkyl chain length, aromatic character and surface charge, directly tunes the balance between hydrophobic, electrostatic and π-π interactions with serum proteins. However, under the tested conditions with PBS, both IgG and HSA depletion efficiencies remained low, highlighting the limited suitability of the designed protocol for effective removal of high-abundance proteins prior to biomarker detection.

To address this limitation, a K_2HPO_4/KH_2PO_4 buffer at 4.68 M was used to enhance protein adsorption by modulating protein solubility through ionic strength. This buffer promoted more efficient protein removal by leveraging both precipitation and adsorption phenomena. As shown in Fig. 3, the use of K_2HPO_4/KH_2PO_4 buffer significantly enhanced the depletion efficiencies in SIL-based SPE,

achieving values exceeding 92%. This improvement is attributed to the synergistic effect between the strong salting-out properties of the K_2HPO_4/KH_2PO_4 buffer and the specific interactions facilitated by each SIL. Under these high ionic strength conditions, protein hydration is reduced and protein-protein interactions are favoured, making both IgG and HSA more susceptible to depletion. In this context, the dominant contribution is likely the salting-out effect promoted by the buffer, while the immobilized IL moieties further contribute to protein removal mainly through electrostatic interactions and hydrophobic effects. Electrostatic interactions are governed by the surface charge of each SIL and the overall charge of the proteins at pH ≈ 7, whereas hydrophobic effects are influenced by the alkyl chain length of the cation. In the activated silica, depletion efficiencies of IgG and HSA were similar to those in the control, indicating no significant adsorption of these proteins to the silica surface. This confirms that non-functionalized silica has negligible impact on protein removal under these conditions and that the improved performance of the SILs arises from the chemical functionality introduced through IL immobilization. These findings point to the potential of ILs as silica-supported ligands, with optimal protein depletion controlled by ionic strength.

The second IL pretreatment approach investigated involved ABS formed by ILs featuring similar chemical structures and properties to those in SILs, using the same buffer (K_2HPO_4/KH_2PO_4 at pH ≈ 7, 4.68 M) and biological matrix (commercial human serum). ILs with alkyl chains longer than butyl were excluded from the ABS study due to their limited solubility in the aqueous phase, which compromises their ability to form stable biphasic systems under the investigated conditions. This criterion is specific to the ABS platform, where ILs act as phase-forming components and must therefore exhibit sufficient water solubility to ensure phase separation with K_2HPO_4/KH_2PO_4 buffer. In contrast, in SPE configurations, the IL is covalently immobilized onto the silica surface and does not participate as a soluble species. Instead, it functions as a surface-confined ligand, where increased hydrophobicity associated with longer alkyl chains can be advantageously exploited to tune surface properties and tailor protein-sorbent interactions. Minor deviations in cation structure relative to the SILs were also introduced due to IL availability. Accordingly, the following imidazolium- and quaternary ammonium-based ILs were studied: $[C_3mim]Cl$, $[N_{2222}]Cl$, $[N_{3333}]Cl$, $[N_{4444}]Cl$, and $[N_{1444}]Cl$ (refer to Table S3 in the Supplementary Material and relevant literature for experimental binodal data (Belchior et al., 2020)).

Fig. 4 depicts the depletion efficiencies of IgG and HSA, expressed as the percentage of protein removed from human serum at the ABS interphase. The respective numerical data is available in the Supplementary Material (Table S4). These results suggest that depletion depends on the IL chemical structure, which shapes system hydrophobicity and the molecular interactions at the interphase driving protein precipitation. IL cations with larger alkyl chains, such as tetrabutylammonium ($[N_{4444}]^+$), lead to more hydrophobic ABS top phases with reduced water content (Rosa et al., 2023). This promotes low protein solubility and stronger protein-protein interactions, while facilitating the salting-out and precipitation of high-abundance proteins like IgG and HSA at the interphase (56 ± 3% and 44 ± 1%, respectively). Conversely, ILs with smaller and more polar cations, such as $[N_{2222}]Cl$, $[N_{3333}]Cl$ or $[C_3mim]Cl$, are more hydrophilic, allowing higher ion hydration, and increased water content in the IL-rich phase. This promotes protein solubilization, thus leading to low or undetectable protein depletion at the interphase (Rosa et al., 2023). Thus, the cationic nature of the ILs here investigated governs the balance between hydrophobicity, hydration, and protein-protein interactions, dictating the effectiveness of ABS in serum pretreatment.

The higher IgG and HSA depletion achieved with SIL-based SPE compared to ABS can be attributed to their distinct operating mechanisms. In SIL-based SPE, protein depletion arises from the combined effect of high buffer ionic strength and direct interactions between serum proteins and the functionalized silica surface, including electrostatic, hydrophobic, van der Waals and, in the case of

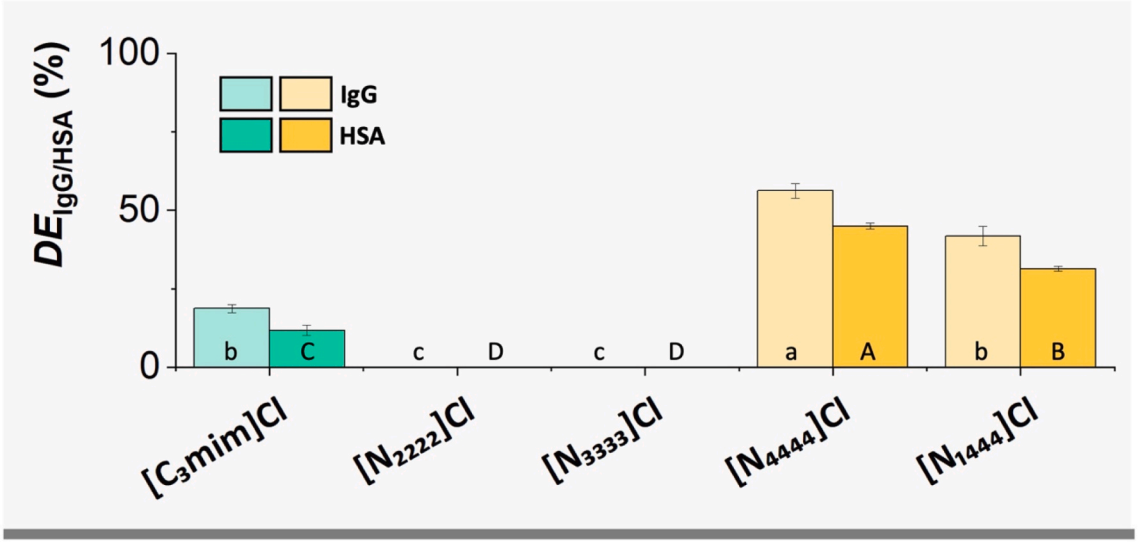

Fig. 4. Depletion efficiencies of IgG (DE_{IgG}, light bars) and HSA (DE_{HSA}, dark bars) obtained via ABS composed of 30 wt% of different ILs, 50 wt% of K_2HPO_4/KH_2PO_4 buffer and 20 wt% of 2-fold diluted human serum. Bars represent mean values, and error bars indicate standard deviation ($n = 3$). Different lowercase letters (IgG) and uppercase letters (HSA) denote statistically significant differences ($p < 0.05$).

imidazolium-based SILs, π-π interactions. In this configuration, SILs act as chemically tunable ligands rather than simple solid supports, promoting effective protein depletion. In contrast, ABS depletion relies on salting-out induced by the K_2HPO_4/KH_2PO_4-rich phase, together with the relative affinity of proteins for each phase and interfacial precipitation phenomena. These processes are strongly governed by IL hydrophobicity, phase hydration and protein accumulation at the interphase. These distinct protein-phase interaction pathways explain the superior performance of SIL-based SPE under the investigated conditions.

Following the identification of SIL-based SPE as the most promising configuration for IgG and HSA depletion, the same optimized experimental conditions (solid-to-liquid ratio, contact time and centrifugation) were applied to commercial human serum, which contains endogenous proteins, salts, metabolites and lipids, spiked with PSA. PSA, a clinically relevant biomarker for prostate cancer and one of the most widely used indicators for its early detection and monitoring, represents an ideal model analyte to validate the practical applicability of SIL-based pretreatment (Walter et al., 2021; Siegel et al., 2025). In clinical practice, total PSA levels below 4 ng mL^{-1} are generally considered within the normal range, whereas values above this threshold warrant further investigation (Descotes, 2019). Concentrations between 4 and 10 ng mL^{-1} define a diagnostic "grey zone", while levels exceeding 10 ng mL^{-1} are associated with an increased risk of prostate cancer (Descotes, 2019). Given that early-stage disease or post-treatment recurrence may involve PSA concentrations in the low ng mL^{-1} range, analytical sensitivity and selectivity are critical, especially for complex matrices like serum (Descotes, 2019).

Fig. 5 shows the recovery yields of serum PSA in the liquid phase, together with the corresponding relative error of analysis (*RE*, %), using SIL-based SPE in the presence of K_2HPO_4/KH_2PO_4 buffer at optimal ionic strength (4.68 M). In addition to SILs, a control without solid phase and activated silica were included to distinguish the contribution of the buffer, the silica support and the immobilized IL moieties. Experiments were conducted at the clinical threshold concentration (4 ng mL^{-1}), aiming to enable accurate PSA quantification while simultaneously removing IgG and HSA via precipitation and/or adsorption onto the SILs to minimize interfering or masking effects. Numerical results are presented in the Supplementary Material (Table S5).

The control experiment suggests that the K_2HPO_4/KH_2PO_4 buffer itself does not compromise PSA isolation/quantification in serum under the tested conditions. However, the use of activated silica led to certain PSA loss in the liquid phase, showing that the non-functionalized silica surface can promote PSA adsorption. This result highlights that silica alone is not sufficiently selective for biomarker-preserving serum pretreatment. In this context, the functionalization of silica with IL moieties was crucial in tailoring interactions between the solid phase and PSA. Among the tested SILs, recovery yields of PSA in the liquid phase ranged from 26 ± 2% to 89 ± 5%, with [Si][N_{3114}]Cl yielding the lowest relative error of analysis (11%). This level of accuracy fulfils a core criterion for clinical bioanalysis, falling within the ±15% range stipulated by the U.S. Food and Drug Administration (FDA) and the European Medicines Agency (EMA) for bioanalytical methods validation (FDA, 2018; EMA, 2019).

Due to its much lower concentration (4 ng mL^{-1}) and smaller molecular weight (34 kDa), PSA poses a distinct separation challenge compared to the high-abundance proteins IgG and HSA, which are present at substantially higher concentrations (16 mg mL^{-1} and

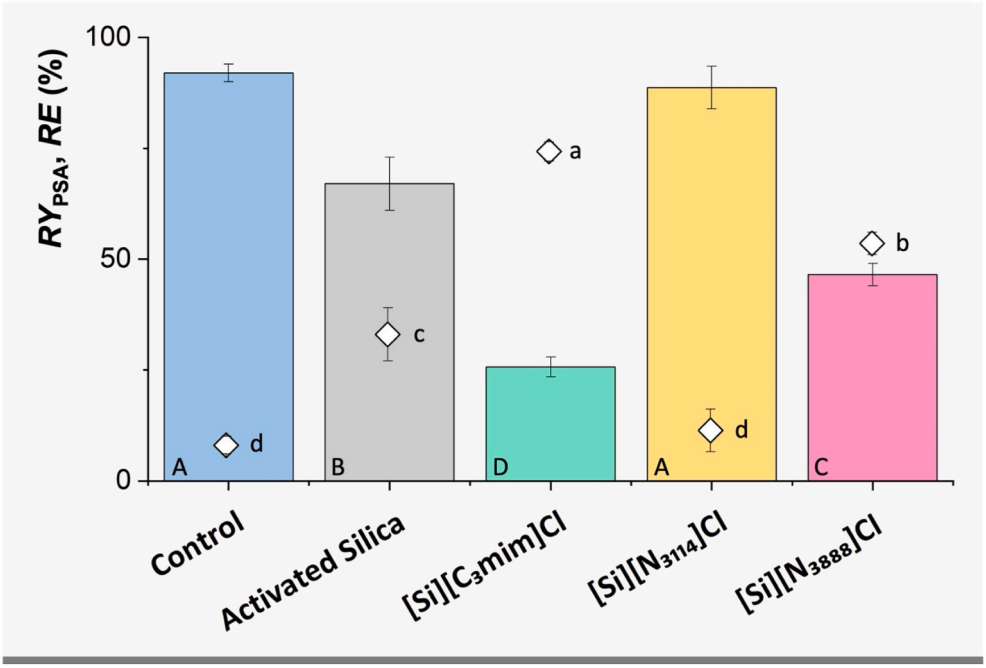

Fig. 5. Recovery yields of PSA in the liquid phase (RY_{PSA}, colored bars), along with the corresponding relative error of analysis (*RE*, white diamonds), obtained via SPE at a solid-to-liquid ratio of 100 mg mL^{-1} with 10-fold diluted human serum spiked with PSA at the 4 ng mL^{-1} cut-off. Control experiments were performed in the absence of silica and SILs. Bars represent mean values, and error bars indicate standard deviation ($n = 3$). Different lowercase letters (*RE*) and uppercase letters (RY_{PSA}) denote statistically significant differences ($p < 0.05$).

50 mg mL^{-1}) with larger molecular weights (150 kDa and 66 kDa, respectively) (Rosa et al., 2023). Consequently, PSA is less likely to precipitate in the presence of strong salting-out agents such as K_2HPO_4/KH_2PO_4 buffer (Rosa et al., 2023). The reduced adsorption of PSA by [Si][N_{3114}]Cl may be ascribed to its shorter methyl chains, which reduce hydrophobic effects toward the biomarker compared to [Si][N_{3888}]Cl (RY_{PSA} of 47 ± 3%). At pH 7, PSA (pI = 6.9) is nearly neutral (Song et al., 2014), while [Si][N_{3114}]Cl (PZC = 9.2), is positively charged, favoring mild electrostatic attraction with negatively charged regions of the biomarker, but limiting retention due to low hydrophobicity. In contrast, [Si][N_{3888}]Cl (PZC = 6.2) is negatively charged at pH 7, potentially leading to electrostatic repulsion. However, its strong hydrophobicity, from three octyl chains, likely drives nonspecific interactions and lowers PSA recovery. [Si][C_3mim]Cl also showed low recovery (26 ± 2%), possibly due to π-π interactions contributing to partial adsorption (Capela et al., 2023). To reinforce the method's feasibility, CD analysis finally confirmed the preservation of PSA's secondary structure post-recovery, in agreement with ELISA results and with spectra matching those obtained in PBS (see Fig. S2 in the Supplementary Material). Overall, PSA recovery in SIL-based SPE is strongly dependent on the IL formulation, indicating distinct contribution of electrostatic interactions and hydrophobicity to biomarker isolation and preservation.

While both IL-based SPE and ABS represent tunable strategies for serum pretreatment, SPE using SILs demonstrated superior performance, achieving >92% depletion of IgG and HSA and 89 ± 5% PSA recovery under optimized conditions. This performance reflects the intrinsic selectivity of the workflow, which is based on the removal of high-abundance serum proteins while preserving low-abundance biomarkers in the liquid phase, even in the presence of endogenous serum interferents, enabling their accurate quantification.

Beyond analytical performance, environmental performance and operational efficiency are increasingly important within Green Analytical Chemistry. Accordingly, two complementary green metrics specifically designed for sample pretreatment were applied to systematically compare both approaches: AGREEprep (Analytical GREEnness metric for sample PREParation) (Wojnowski et al., 2022) and the Sample Preparation Metric of Sustainability (SPMS) (González-Martín et al., 2023b). AGREEprep provides a criterion-based score between 0 and 1 derived from ten green sample preparation principles addressing safety, sustainability, efficiency, waste,

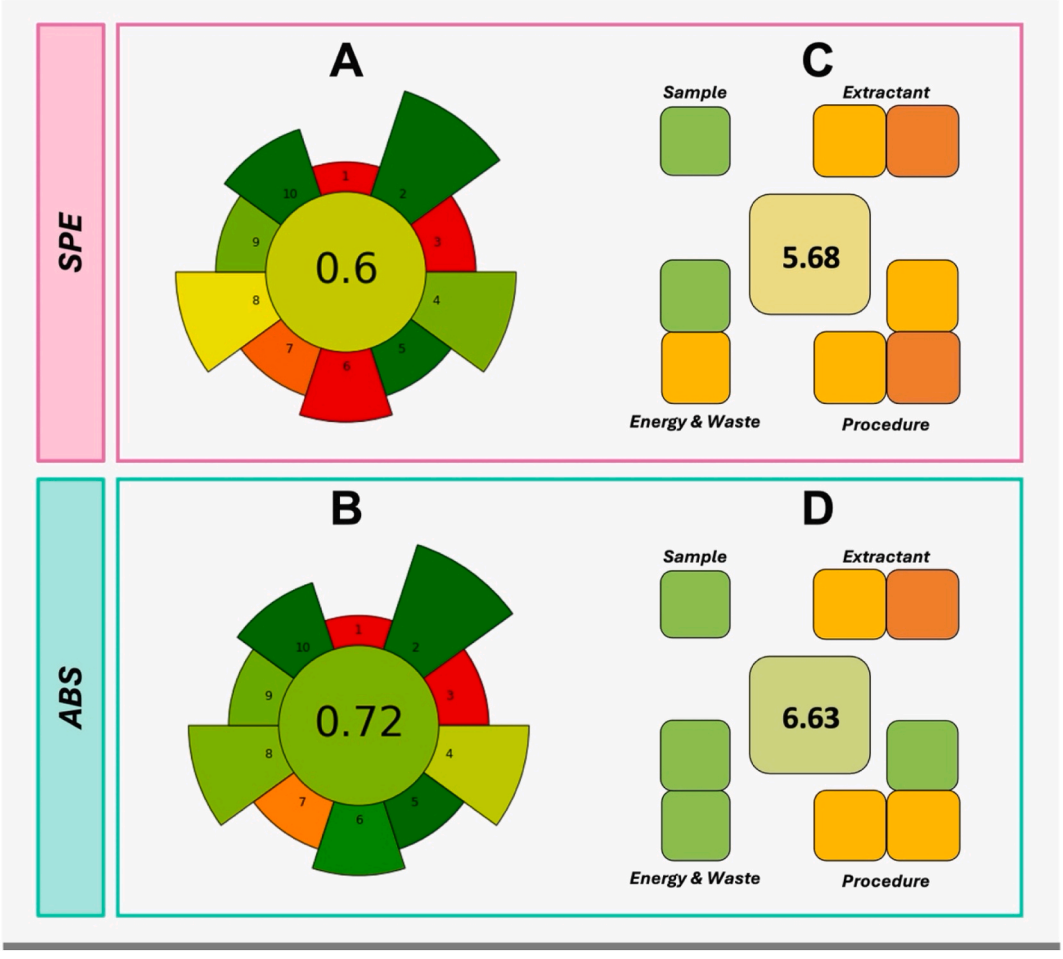

Fig. 6. Assessment of IL-based serum pretreatment strategies by green metrics. AGREEprep evaluation for SIL-based SPE (A) and IL-based ABS (B); SPMS evaluation for SIL-based SPE (C) and IL-based ABS (D).

and energy consumption. SPMS delivers a numerical sustainability score based on nine parameters covering sample requirements, extractant characteristics, procedural complexity, and resource consumption, including energy use and waste generation. The corresponding metric diagrams and numerical evaluations are summarized in Fig. 6.

Application of the AGREEprep metric (Fig. 6A and B) resulted in overall scores of 0.6 for the SIL-based SPE strategy and 0.72 for the IL-based ABS approach, indicating comparable and moderately high levels of green analytical performance. Both methods scored poorly in criterion 1 (sample preparation placement) due to their ex-situ operation, whereas maximum scores were obtained for criterion 2 (hazardous materials) and criterion 10 (operator safety), reflecting the absence of toxic or hazardous reagents. Criterion 3 (sustainability, renewability, and reusability of materials) also received low scores for both approaches, as the materials employed are neither renewable nor reused. Both approaches were considered single-use workflows due to the use of human serum as a complex biological matrix, which may lead to protein fouling, biomolecule carryover, and potential cross-contamination, limiting practical reusability under the conditions studied. In SPE, IL moieties are covalently immobilized on silica, improving handling stability and reducing leaching, whereas in ABS the ILs act as phase-forming components and are not recovered after use.

Differences between the two strategies were mainly governed by operational parameters. SPE exhibited superior performance in criterion 5 (size economy of the sample) and criterion 4 (waste generation), requiring lower serum amounts and producing reduced aqueous waste compared to ABS. In contrast, ABS achieved higher scores in criterion 6 (sample throughput), criterion 7 (integration and automation), and criterion 8 (energy consumption), mainly due to a more expedited pretreatment workflow. ABS requires a single centrifugation step, whereas the SIL-based SPE protocol involves an additional agitation step followed by longer centrifugation. This reduced number of handling steps enables higher throughput, and results in a lower operational energy demand. Both strategies obtained identical scores for criterion 9 (post-sample preparation configuration for analysis), as the prepared samples are designed to be compatible with common bioanalytical detection platforms, such as immunoassays (e.g., ELISA), in line with established clinical practices.

These trends are further corroborated by the SPMS evaluation (Fig. 6C and D), which yielded overall scores of 5.68 for the SIL-based SPE strategy and 6.63 for the IL-based ABS approach, confirming the higher operational efficiency of ABS and the lower material and waste footprint of SPE. Overall, the combined AGREEprep and SPMS assessments reveal a clear trade-off between environmental performance and analytical efficiency. While ABS favor process integration, throughput, and energy efficiency, SPE provides superior material economy, waste minimization and higher depletion of high-abundance proteins, which is critical for reliable trace-level biomarker analysis, such as PSA. These differences support SIL-based SPE and IL-based ABS as complementary rather than interchangeable serum pretreatment platforms, with performance governed by both IL chemical structure and mode of system integration.

To complement this green analytical benchmarking and compare the proposed approaches with existing IL-based sample pretreatment strategies, Table 1 summarizes representative methods reported in the literature. ILs have been integrated into different pretreatment formats, ranging from their use as mobile extraction solvents in liquid-phase microextraction systems to their role as phase-forming components or adjuvants in ABS, and as immobilized ligands in SPE.

An overall pattern emerges, where simple configurations such as IL-based liquid-phase microextraction, typically based on hydrophobic, water-immiscible ILs, provide fast and low-solvent workflows but are limited by selectivity, structural tunability and toxicity-related concerns (De et al., 2019; Cheng et al., 2008; vaezzadeh et al., 2010). In contrast, polymer-salt ABS with ILs as adjuvants enhance operational performance at the expense of increased compositional complexity (Rosa et al., 2023), while magnetic IL-based approaches enable rapid separation and simplified handling but raise concerns related to material complexity and hydrolytic stability (Emaus et al., 2019; Abdallah et al., 2022; Emaus and Anderson, 2020). IL-based ABS offer simplified workflows and low energy demand, although achieving an optimal balance between protein depletion efficiency and biomarker recovery remains

Table 1
Comparison of IL-based sample pretreatment strategies in terms of integration modes, separation mechanisms, analytical performance, and green and operational trade-offs.

IL integration strategy	Pretreatment configuration	Main mechanism	Green/operational profile	Main analytical focus	Ref.
ILs as extraction solvents	IL-based liquid-phase microextraction	Partition between immiscible phases	Low solvent use and rapid extraction, but limited tunability and toxicity concerns	Analyte extraction, preconcentration and protein depletion	(De et al., 2019; Cheng et al., 2008; vaezzadeh et al., 2010)
Magnetic ILs	Magnetic IL-based extraction	Magnetically assisted separation	Rapid separation and simple handling, but material complexity and stability issues	Analyte extraction and preconcentration	(Emaus et al., 2019; Abdallah et al., 2022; Emaus and Anderson, 2020)
ILs as adjuvants	Polymer-salt IL-assisted ABS	Partition and interfacial precipitation	Tunable performance, but higher system complexity	Protein depletion and biomarker recovery	Rosa et al. (2023)
ILs as phase-forming components	IL-based ABS	Partition and interfacial precipitation	Low energy demand and simplified workflow, but challenging depletion-recovery balance	Protein depletion and biomarker recovery	(Rosa et al., 2023), this work
ILs immobilized on silica supports (SILs)	SIL-based SPE	Surface-confined interactions combined with salting-out effects	Reduced waste and high selectivity, but more complex workflow	Protein depletion and biomarker isolation	This work

challenging (Rosa et al., 2023). Experimentally, this was reflected in lower protein depletion observed for IL-based ABS under the tested conditions, consistent with a bulk partition-driven mechanism. Still, their operational advantages make them attractive for rapid pretreatment scenarios where extensive depletion is not required.

Finally, immobilized ILs (SILs) are well suited for targeted protein depletion and biomarker isolation, particularly in applications requiring high analytical selectivity and analyte integrity. This is supported by the performance obtained with [Si][N_{3114}]Cl, mediated by salting-out and direct protein-sorbent interactions. Despite requiring a more complex workflow due to surface functionalization and additional processing steps, SIL-based SPE stands out as an environmentally favourable IL-based pretreatment approach, ensuring efficient performance in both high-abundance protein depletion and biomarker isolation.

4. Conclusions

This work provides a direct comparison between IL-based SPE and ABS strategies for efficient serum pretreatment and improved biomarker analysis, marking a key advancement in Green Analytical Chemistry-guided sample preparation. The integration of SILs into SPE enabled a highly selective approach, achieving >92% depletion of IgG and HSA and 89% recovery of PSA, with a relative error of 11%, within acceptable ranges for bioanalytical applications and prostate cancer biomarker detection. Green metric evaluation of the SIL-based SPE approach using AGREEprep and SPMS further confirmed its strong consistency with Green Analytical Chemistry principles and favourable analytical performance in sample preparation. The results highlight the relevance of IL-based strategies within Green Analytical Chemistry and their contribution to addressing United Nations Sustainable Development Goals 3, 9 and 12 through improved analytical performance, methodological innovation, and reduced consumption of reagents and materials. Ultimately, this work supports the development of high-performance bioanalytical workflows with potential applicability in clinically relevant settings.

CRediT authorship contribution statement

Maria S.M. Mendes: Data curation, Formal analysis, Investigation, Methodology, Validation, Visualization, Writing – original draft. **Hugo Santos:** Data curation, Investigation. **Inês Cruz:** Formal analysis, Investigation. **Márcia C. Neves:** Methodology, Supervision, Writing – review & editing. **Mara G. Freire:** Conceptualization, Funding acquisition, Supervision, Writing – review & editing. **Francisca A. e Silva:** Conceptualization, Funding acquisition, Project administration, Supervision, Writing – review & editing.

Declaration of competing interest

The authors declare that they have no known competing financial interests or personal relationships that could have appeared to influence the work reported in this paper.

Acknowledgements

This work was developed within the scope of the project CICECO Aveiro Institute of Materials, UID/50011/2025 (DOI: https://doi.org/10.54499/UID/50011/2025) & LA/P/0006/2020 (DOI: https://doi.org/10.54499/LA/P/0006/2020), financed by national funds through the FCT/MCTES (PIDDAC). This work was developed within the project ILSurvive, PTDC/EMD-TLM/3253/2020 (DOI: https://doi.org/10.54499/PTDC/EMD-TLM/3253/2020), funded by national funds (OE), through FCT/MCTES. M.S.M.M. and I.C. acknowledge FCT for the doctoral grants 2022.11229.BD (DOI: https://doi.org/10.54499/2022.11229.BD) and 2024.06707.BD (DOI: https://doi.org/10.54499/2024.06707.BD), respectively. F.A.eS. acknowledges FCT for the Scientific Employment Stimulus researcher contract CEECIND/03076/2018/CP1559/CT0024 (DOI: https://doi.org/10.54499/CEECIND/03076/2018/CP1559/CT0024).

Appendix A. Supplementary data

Supplementary data to this article can be found online at https://doi.org/10.1016/j.scp.2026.102475.

Data availability

Data will be made available on request.

References

Abdallah, I.A., Hammad, S.F., Bedair, A., Abdelaziz, M.A., Danielson, N.D., Elshafeey, A.H., Mansour, F.R., 2022. A gadolinium-based magnetic ionic liquid for supramolecular dispersive liquid–liquid microextraction followed by HPLC/UV for the determination of favipiravir in human plasma. Biomed. Chromatogr. 36. https://doi.org/10.1002/bmc.5365.

Areekal, N.N., Boravelli, J.A.R., Raghavarao, K.S.M.S., Vir, A.B., 2025. Aqueous two-phase systems: methods of binodal curve generation and applications. Adv. Colloid Interface Sci. 339, 103418. https://doi.org/10.1016/j.cis.2025.103418.

Belchior, D.C.V., Quental, M.V., Pereira, M.M., Mendonça, C.M.N., Duarte, I.F., Freire, M.G., 2020. Performance of tetraalkylammonium-based ionic liquids as constituents of aqueous biphasic systems in the extraction of ovalbumin and lysozyme. Sep. Purif. Technol. 233, 116019. https://doi.org/10.1016/j.seppur.2019.116019.

Bernardo, S.C., Araújo, B.R., Sousa, A.C.A., Barros, R.A., Cristovão, A.C., Neves, M.C., Freire, M.G., 2020. Supported ionic liquids for the efficient removal of acetylsalicylic acid from aqueous solutions. Eur. J. Inorg. Chem. 2020, 2380–2389. https://doi.org/10.1002/ejic.202000101.

Brudar, S., Hribar-Lee, B., 2021. Effect of buffer on protein stability in aqueous solutions: a simple protein aggregation model. J. Phys. Chem. B 125, 2504–2512. https://doi.org/10.1021/acs.jpcb.0c10339.

Capela, E.V., Bairos, J., Pedro, A.Q., Neves, M.C., Raquel Aires-Barros, M., Azevedo, A.M., Coutinho, J.A.P., Tavares, A.P.M., Freire, M.G., 2023. Supported ionic liquids as customizable materials to purify immunoglobulin G. Sep. Purif. Technol. 305. https://doi.org/10.1016/j.seppur.2022.122464.

Cheng, D., Chen, X., Shu, Y., Wang, J., 2008. Selective extraction/isolation of hemoglobin with ionic liquid 1-butyl-3-trimethylsilylimidazolium hexafluorophosphate (BtmsimPF6). Talanta 75, 1270–1278. https://doi.org/10.1016/j.talanta.2008.01.044.

De Boeck, M., Moreels, L., Dehaen, W., Tytgat, J., Cuypers, E., 2019. Evaluation of the suitability of ionic liquid-based liquid-liquid microextractions for blood protein removal. J. Pharm. Biomed. Anal. 164, 57–61. https://doi.org/10.1016/j.jpba.2018.10.019.

Descotes, J.-L., 2019. Diagnosis of prostate cancer. Asian J. Urol. 6, 129–136. https://doi.org/10.1016/j.ajur.2018.11.007.

EMA, ICH guideline M10 on bioanalytical method validation and study sample analysis, EMA/CHMP/ICH/172948/2019: https://www.ema.europa.eu/en/documents/scientific-guideline/ich-guideline-m10-bioanalytical-method-validation-step-5_en.pdf (accessed July 15, 2025).

Emaus, M.N., Varona, M., Anderson, J.L., 2019. Sequence-specific preconcentration of a mutation prone KRAS fragment from plasma using ion-tagged oligonucleotides coupled to qPCR compatible magnetic ionic liquid solvents. Anal. Chim. Acta 1068, 1–10. https://doi.org/10.1016/j.aca.2019.04.005.

Emaus, M.N., Anderson, J.L., 2020. Simultaneous cell lysis and DNA extraction from whole blood using magnetic ionic liquids. Anal. Bioanal. Chem. 412, 8039–8049. https://doi.org/10.1007/s00216-020-02941-w.

FDA, Bioanalytical Method Validation, 05/24/18: https://www.fda.gov/files/drugs/published/Bioanalytical-Method-Validation-Guidance-for-Industry.pdf (accessed July 15, 2025).

Gałuszka, A., Migaszewski, Z., Namieśnik, J., 2013. The 12 principles of green analytical chemistry and the significance mnemonic of green analytical practices. TrAC, Trends Anal. Chem. 50, 78–84. https://doi.org/10.1016/j.trac.2013.04.010.

González-Martín, R., e Silva, F.A., Trujillo-Rodríguez, M.J., Díaz Díaz, D., Lorenzo-Morales, J., Freire, M.G., Pino, V., 2023a. Ionic liquid-based aqueous biphasic systems as one-step clean-up, microextraction and preconcentration platforms for the improved determination of salivary biomarkers. Green Chem. 25, 8544–8557. https://doi.org/10.1039/d3gc02046k.

González-Martín, R., Gutiérrez-Serpa, A., Pino, V., Sajid, M., 2023b. A tool to assess analytical sample preparation procedures: sample preparation metric of sustainability. J. Chromatogr. A 1707, 464291. https://doi.org/10.1016/j.chroma.2023.464291.

Han, Q., Su, Y., Smith, K.M., Binns, J., Drummond, C.J., Darmanin, C., Greaves, T.L., 2023. Probing ion-binding at a protein interface: modulation of protein properties by ionic liquids. J. Colloid Interface Sci. 650, 1393–1405. https://doi.org/10.1016/j.jcis.2023.07.045.

Issaq, H.J., Veenstra, T.D., 2020. Sample depletion, fractionation, and enrichment for biomarker discovery. In: Proteomic and Metabolomic Approaches to Biomarker Discovery. Elsevier, pp. 95–102. https://doi.org/10.1016/B978-0-12-394446-7.00015-7.

Kirkland, J.J., van Straten, M.A., Claessens, H.A., 1995. High pH mobile phase effects on silica-based reversed-phase high-performance liquid chromatographic columns. J. Chromatogr. A 691, 3–19. https://doi.org/10.1016/0021-9673(94)00631-I.

López-Lorente, Á.I., Pena-Pereira, F., Pedersen-Bjergaard, S., Zuin, V.G., Ozkan, S.A., Psillakis, E., 2022. The ten principles of green sample preparation. TrAC, Trends Anal. Chem. 148, 116530. https://doi.org/10.1016/j.trac.2022.116530.

Mota-Martinez, M.T., Brandl, P., Hallett, J.P., Mac Dowell, N., 2018. Challenges and opportunities for the utilisation of ionic liquids as solvents for CO2 capture. Mol. Syst. Des. Eng. 3, 560–571. https://doi.org/10.1039/c8me00009c.

Qiu, H., Jiang, S., Liu, X., 2006. N-Methylimidazolium anion-exchange stationary phase for high-performance liquid chromatography. J. Chromatogr. A 1103, 265–270. https://doi.org/10.1016/j.chroma.2005.11.035.

Rosa, M.E., Mendes, M.S.M., Carmo, E., Conde, J.P., Coutinho, J.A.P., Freire, M.G., e Silva, F.A., 2023. Tailored pretreatment of serum samples and biomarker extraction afforded by ionic liquids as constituents of aqueous biphasic systems. Sep. Purif. Technol. 322, 124248. https://doi.org/10.1016/j.seppur.2023.124248.

Rosa, P.A.J., Azevedo, A.M., Ferreira, I.F., de Vries, J., Korporaal, R., Verhoef, H.J., Visser, T.J., Aires-Barros, M.R., 2007. Affinity partitioning of human antibodies in aqueous two-phase systems. J. Chromatogr. A 1162, 103–113. https://doi.org/10.1016/j.chroma.2007.03.067.

Siegel, R.L., Kratzer, T.B., Giaquinto, A.N., Sung, H., Jemal, A., 2025. Cancer statistics, 2025. CA Cancer J. Clin. 75, 10–45. https://doi.org/10.3322/caac.21871.

Sim, S.-L., He, T., Tscheliessnig, A., Mueller, M., Tan, R.B.H., Jungbauer, A., 2012. Protein precipitation by polyethylene glycol: a generalized model based on hydrodynamic radius. J. Biotechnol. 157, 315–319. https://doi.org/10.1016/j.jbiotec.2011.09.028.

Song, E., Mayampurath, A., Yu, C.-Y., Tang, H., Mechref, Y., 2014. Glycoproteomics: identifying the glycosylation of prostate specific antigen at normal and high isoelectric points by LC–MS/MS. J. Proteome Res. 13, 5570–5580. https://doi.org/10.1021/pr500575r.

vaezzadeh, M., Shemirani, F., Majidi, B., 2010. Microextraction technique based on ionic liquid for preconcentration and determination of palladium in food additive, sea water, tea and biological samples. Food Chem. Toxicol. 48, 1455–1460. https://doi.org/10.1016/j.fct.2010.03.005.

Walter, S.D., Hu, J., Talala, K., Tammela, T., Taari, K., Auvinen, A., 2021. Estimating the rate of overdiagnosis with prostate cancer screening: evidence from the Finnish component of the european randomized study of screening for prostate cancer. Cancer Causes Control 32, 1299–1313. https://doi.org/10.1007/s10552-021-01480-8.

Wang, Y., Zhao, W., Gao, R., Heinlein, J.A., Pfefferle, L.D., Hussain, S., Zhang, J., Wang, X., An, J., 2023. Facile and green preparation of multifeatured montmorillonite-supported $Fe3O_4$ -Cu^{2+} hybrid magnetic nanomaterials for the selective adsorption of a high-abundance protein from complex biological matrices. Green Chem. 25, 3705–3714. https://doi.org/10.1039/D2GC04546J.

Wojnowski, W., Tobiszewski, M., Pena-Pereira, F., Psillakis, E., 2022. AGREEprep – analytical greenness metric for sample preparation. TrAC, Trends Anal. Chem. 149, 116553. https://doi.org/10.1016/j.trac.2022.116553.

Zeger, V.R., Thapa, B., Shamsaei, D., DeLair, J.F., Taylor, T.L., Anderson, J.L., 2025. Ionic liquids in analytical chemistry: fundamentals, technological advances, and future outlook. Anal. Chem. 97, 4793–4818. https://doi.org/10.1021/acs.analchem.5c00264.